Surface Chemistry

DOI: 10.1002/anie.200903403

Bridging the Gap between CO Adsorption Studies on Gold Model Surfaces and Supported Nanoparticles**

*Miguel López-Haro, Juan J. Delgado, José M. Cies, Eloy del Rio, Serafin Bernal, Robbie Burch, Miguel A. Cauqui, Susana Trasobares, José A. Pérez-Omil, Pascale Bayle-Guillemaud, and José J. Calvino**

An in-depth understanding of CO adsorption on highly dispersed gold nanoparticles (AuNPs) is critically important to fully interpret the catalytic behavior of supported gold systems in processes such as CO oxidation,[1–4] PROX (selective oxidation of CO in presence of a large excess of H_2),[5–7] or LT-WGS (low-temperature water gas-shift)[8–10] reactions. Despite its relevance, the quantitative data and fundamental information presently available on the CO–Au interaction mainly comes from studies carried out on model single-crystal and thin-film surfaces under experimental conditions far from those at which catalytic assays on supported gold systems are typically run.[10–14] Probably because of the very weak and singular nature of the CO–Au interaction, which on the basis of both theoretical[15,16] and experimental[17,18] studies is generally acknowledged to take place on low-coordination surface sites, and the additional contribution of the support,[19] a few studies have been carried out that were aimed at estimating the amount of CO adsorbed at low temperature on powdered[20,21] or model[22–24] supported AuNPs. To our knowledge, however, none of these have arrived at a detailed quantitative description of this process under conditions close to those occurring in real catalytic reactions.

To bridge this gap, we have developed an approach in which AuNP size distributions, as determined from HAADF-STEM (high-angle annular dark-field scanning transmission electron microscopy) and quantitative CO adsorption data, as determined from volumetric adsorption at 308 K, under CO partial pressures ranging from 6.65×10^2 Pa to 3.99×10^4 Pa, are jointly analyzed with the help of a nanostructural model for the gold particles. This model could be deduced from the analysis of images recorded in a parallel HRTEM (high-resolution transmission electron microscopy) study. As discussed herein, this approach gives a substantial experimental support to the extension to supported gold catalysts of the chemical principles governing the CO adsorption on model surfaces.

We investigated two catalyst samples, 2.5 wt% Au/$Ce_{0.62}Zr_{0.38}O_2$ (Au/CZ) and 1.5 wt% Au/$Ce_{0.50}Tb_{0.12}Zr_{0.38}O_{2-x}$ (Au/CTZ), which have significantly different gold particle size distributions. Two consecutive CO volumetric adsorption isotherms were recorded on the gold catalysts and the corresponding supports. Prior to running the second isotherms, samples were evacuated (residual pressure $P_{res} < 1.33\times10^{-4}$ Pa) for 30 min at 308 K. By processing the volumetric data in a similar way to earlier studies[19] (for details, see the Supporting Information), the amounts of CO adsorbed on the AuNPs, on the surface cations of the supports (weak adsorption), and on the surface anions of the supports, which mainly consist of strongly chemisorbed carbonate species,[19] could be determined from the difference of the two isotherms. The amount of CO adsorbed on the AuNPs at $P_{CO} = 1.33\times10^4$ Pa (100 Torr) was used as a measurement of the saturation coverage. The corresponding data are reported in Table 1 and the Supporting Information, Figure S1.

Gold particle size distributions were determined for each of the investigated catalysts from the analysis of series of experimental ultra-high-resolution HAADF-STEM images (Supporting Information, Figure S2). In accordance with the physical principles lying behind the mechanism of image formation,[25] this technique is particularly suitable for obtaining reliable metal particle size distributions in oxide-supported metal catalysts.[26–30] Moreover, as recently shown,[31] this technique can be fruitfully applied to a very fine characterization of AuNPs dispersed on mixed oxides of heavy elements, as is the case of those investigated herein. (Size distributions for Au/CZ and Au/CTZ catalysts are shown in the Supporting Information, Figure S2).

[*] M. López-Haro, Dr. J. J. Delgado, J. M. Cies, E. del Rio, S. Bernal, Dr. M. A. Cauqui, Dr. S. Trasobares, Dr. J. A. Pérez-Omil, Dr. J. J. Calvino
Departamento de Ciencia de los Materiales e Ingeniería Metalúrgica y Química Inorgánica
Facultad de Ciencias, Universidad de Cádiz
Campus Rio San Pedro, 11510-Puerto Real, Cádiz (Spain)
Fax: (+34) 956-016-288
E-mail: jose.calvino@uca.es
Prof. R. Burch
Center for the Theory and Application of Catalysis (CenTaCat)
School of Chemistry and Chemical Engineering
Queen's University Belfast, Belfast, BT9 5AG (UK)
Dr. P. Bayle-Guillemaud
CEA Grenoble,INAC/SP2M
17 Rue de Martyres, 38054 Grenoble (France)

[**] Financial support from MICIIN-Spain/FEDER-EU (Project MAT2008-00889-NAN), the Junta de Andalucía (Groups FQM-110 and FQM-334), and the EU (Contract 025995 (RITA) CENTACAT) is acknowledged. The starting Ce/Zr and Ce/Tb/Zr mixed-oxide samples used in this work were kindly donated by Grace Davison. S.T. acknowledges the Ramón y Cajal contract. M.L.H., J.M.C. and E.R. are grateful to MICINN for supporting their doctorate grants. TEM/STEM data were acquired at the UHR-HAADF-STEM facilities at CEA Grenoble and at DME SCCyT of UCA.

Supporting information for this article is available on the WWW under http://dx.doi.org/10.1002/anie.200903403.

Table 1: Comparison of experimental CO/Au_T and CO/Au_S data with the dispersion parameters D_j and D_{4-j}.[a]

Catalyst	V_{ads} (CO/Au_T)	D_4 (D_{4-4})	D_5 (D_{4-5})	D_6 (D_{4-6})	D_7 (D_{4-7})	D_8 (D_{4-8})	D_9 (D_{4-9})	D_p
Au/CTZ	0.13	0.00 (*0.00*)	0.02 (*0.02*)	0.05 (*0.07*)	0.07 (*0.14*)	0.02 (*0.16*)	0.13 (*0.29*)	0.06
Au/CZ	0.49	0.02 (*0.02*)	0.07 (*0.09*)	0.17 (*0.26*)	0.22 (*0.48*)	0.01 (*0.49*)	0.20 (*0.69*)	0.17
Catalyst	V_{ads} (CO/Au_S)	CN_4 (CN_{4-4})	CN_5 (CN_{4-5})	CN_6 (CN_{4-6})	CN_7 (CN_{4-7})	CN_8 (CN_{4-8})	CN_9 (CN_{4-9})	P
Au/CTZ	0.46	0.00 (*0.00*)	0.07 (*0.07*)	0.17 (*0.24*)	0.24 (*0.48*)	0.07 (*0.55*)	0.45 (*1.00*)	0.20
Au/CZ	0.73	0.03 (*0.03*)	0.10 (*0.13*)	0.25 (*0.38*)	0.32 (*0.70*)	0.01 (*0.71*)	0.29 (*1.00*)	0.25

[a] Values determined from volumetric adsorption V_{ads}, and the fraction of the total number of surface gold atoms with a pre-established coordination number, CN = *j*, or CN values ranging from 4 to *j* (*j* = 4–9).

Catalysts were also characterized by high-resolution electron microscopy (HREM). As deduced from the micrograph (Figure 1), a truncated cuboctahedron morphology

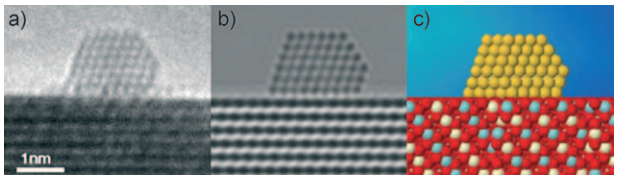

Figure 1. AuNP used as a model in the metal dispersion studies. a) HREM image for the Au/CTZ sample, b) computer-simulated image, and c) nanostructural model used as the input to calculate image (b).

may be considered as an appropriate model for our AuNPs. Accordingly, the analysis of the experimental size distributions (Supporting Information, Figure S2) was performed on the basis of a set of truncated cuboctahedron shaped particles; the sizes were increased in discrete steps to cover the whole range of particle sizes found in the experimental distributions. Some of these model particles are shown in Figure 2. Along with perfect cuboctahedron particles, we have been able to model some slightly distorted morphologies, which were generated by an extra growth of some of their facets. In this way, the sizes included in our set of particles could be widened, and therefore a finer analysis of the experimental results could be performed. Moreover, the inclusion of distorted morphologies has allowed us to account for geometries actually observed in real metal particles.

By applying this nanostructural model to the experimental size distributions (Supporting Information, Figure S2), the total metal dispersion, $D = Au_S/Au_T$, where Au_S = total number of surface gold atoms, and Au_T = total number of gold atoms, could be determined for Au/CZ ($D = 0.69$) and Au/CTZ catalysts ($D = 0.29$). The number of counted metal particles was large enough to allow an estimate of D values with accuracy better than 2% (procedure given in the Supporting Information, Figure S3).

By using the full set of model AuNPs (such as in Figure 2a), a much more detailed analysis of the metal dispersion data can be performed. It is possible to estimate the contribution to the total dispersion of the surface gold atoms showing any of the coordination numbers (*j*) found in the modeled particles (*j* = 3–9). The estimate of these D_j values, where $D_j = Au_{S,j}/Au_T$, was made with the help of a computer program that we have developed. In the case of the metal–support interface, we could count the gold atoms located exclusively at the perimeter of the particles. Similarly, if we use

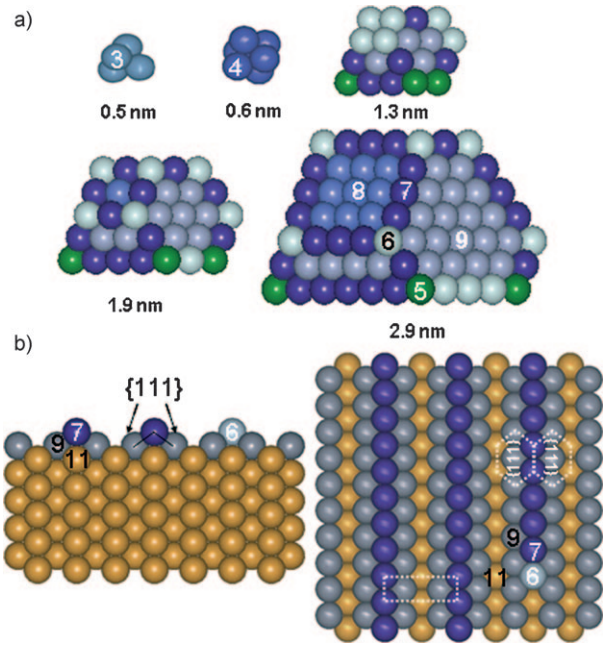

Figure 2. a) Some model AuNPs of the whole set used in the D_{4-j} analysis. Coordination numbers of surface atoms is indicated. Both perfect cuboctahedron and slightly distorted morphologies are included in our set. b) Structural model of the Au {111}–1×2, missing row, reconstructed surface. Two orthogonal views are shown.

as input the whole set of previously determined D_j values (Table 1), we may easily calculate the cumulative contribution to the total dispersion of surface gold atoms with CN ranging from the lowest one, *j* = 4, to any other *j* value, D_{4-j} (*j* = 4–9).

Two additional relevant parameters may also be determined: the fraction of the total number of gold surface atoms with a pre-established coordination number, CN_j (*j* = 4–9), and the corresponding cumulative data, CN_{4-j}, that is, the fraction of the total surface atoms with CN ranging from 4 to *j* (*j* = 4–9). CN_j and CN_{4-j} data for Au/CZ and Au/CTZ catalysts is also given in Table 1.

A number of conclusions may be drawn from the analysis of Table 1 (see also the Supporting Information, Figure S4, in

which the evolution of D_{4-j} against j ($j=4$–9) is plotted). As deduced from the reported D_{4-9} values for Au/CTZ (0.29) and Au/CZ (0.69), the surface atoms represent one third and two thirds of the total gold atoms in the catalysts, respectively. Similarly, the frequency of observation of surface gold atoms with coordination number ranging from 4 to 9, CN_j, are remarkably different. The relative weight of surface atoms with low CN ($j \leq 7$) is significantly larger on Au/CZ. The opposite is true for atoms showing the highest coordination numbers, $j \geq 8$, for which the relative weight is larger on the Au/CTZ catalyst. These observations clearly reflect the different particle size distribution exhibited by both samples. Furthermore, D_{4-j} values sharply increase with the inclusion of surface atoms with the highest coordination number, $j=9$, on both catalysts (Supporting Information, Figure S4). A further important point is that the experimental CO/Au_T data are in very good agreement with those determined for D_{4-7} (Table 1 and the Supporting Information, Figure S4). This agreement shows that, under the experimental conditions of our volumetric studies, the apparent saturation of the AuNPs is reached when surface gold atoms with coordination number $j \leq 7$ are the only ones involved in the CO adsorption process. Similarly, gold atoms with $CN=9$, that is, those present in {111} facets, do not adsorb any CO; otherwise, a very significant increase in the CO/Au_T ratio should be expected to occur (Supporting Information, Figure S4). Den Breejen et al. have reported similar results in a detailed study of CO adsorption on cobalt nanoparticles.[32]

Regarding the gold atoms with $CN=8$, that is, those corresponding to {100} facets, the data obtained for Au/CTZ (Table 1 and the Supporting Information, Figure S4) strongly suggest that they are not involved in the CO adsorption process. In contrast, in the case of the Au/CZ catalyst, no conclusive answer can be given because of the negligible contribution of these atoms to the total number of surface sites ($CN_8=0.01$). However, as predicted by our approach, their contribution to CO/Au_T, if any, would certainly be within the experimental error in CO adsorption measurements.

The computer program has also allowed us to estimate the contribution of gold atoms located in the perimeter of the metal–support interface (Au_P) to the total dispersion D_p ($D_p = Au_P/Au_T$), and also to the total surface atoms, P ($P = Au_P/Au_S$). This information is relevant because, as a number of authors have stressed,[33] these specific sites may play a key role in determining the catalytic behavior of the supported AuNPs. Also noticeable is the fact that the D_p values for Au/CZ (0.17) and Au/CTZ (0.06) are far lower than the experimental CO/Au_T ratios (0.49 for Au/CZ and 0.13 for Au/CTZ). Accordingly, CO adsorption results cannot be interpreted in terms of a specific interaction exclusively involving the perimeter gold atoms.

As already commented upon, the quantitative information and chemical principles underlying the CO–Au interactions mainly come from studies carried out on model surfaces. Therefore, it would be of interest to compare the results presented and discussed herein for two supported catalysts with those available in the literature for a gold surface model sample.

Figure 2b depicts the structure of a Au{110} 1×2 reconstructed surface. It can be considered as a {111}-microfaceted surface. As deduced from the unit cell marked on Figure 2b, atoms with $CN=7$ represent one fourth of the total surface atoms, those with $CN=9$ one half of them, with the remaining 25% having $CN=11$. In accordance with the experimental CO adsorption studies reported by Goodman et al. on this model surface, the saturation coverage is reached at $CO/Au_S=0.30$.[12] Therefore, the surface atoms mainly involved in CO adsorption are those showing the lowest coordination number, $j=7$. The slight excess of chemisorbed CO with respect to the surface concentration of seven-coordinate atoms, 0.25, is interpreted[12] as being due to the existence of a small density of steps along the ⟨110⟩ direction, with inherent creation of six-coordinate sites (Figure 2b).

Some clear analogies may be established between the structure of this reconstructed surface and that exhibited by the supported AuNPs in our catalysts (Figure 2a). Both surfaces show {111}-crossing facets of nanosize dimensions leading to the formation of edges populated by seven-coordinate gold atoms. In the case of the supported catalysts, however, sites with lower coordination number (4–6) also occur. As revealed by the CN_j and CN_{4-j} data (Table 1), their relative contribution to the total number of surface atoms, though sensitive to the specific particle size distribution exhibited by the catalysts, is very significant on both samples, and represents up to 24% ($CN_{4-6}=0.24$) of the total surface atoms in the Au/CTZ catalyst, and 38% ($CN_{4-6}=0.38$) in the Au/CZ sample.

The principles governing the CO adsorption on model surfaces could therefore be reasonably extended to supported catalysts. The major difference is the contribution to the total amount of chemisorbed CO of the atoms with low coordination numbers, which can only occur on the supported catalysts. As a result, the fraction of the total number of surface sites involved in CO adsorption is significantly smaller on model single-crystal surfaces (0.30) than on our supported catalysts ($CN_{4-7}=0.48$ for Au/CTZ and $CN_{4-7}=0.71$ for Au/CZ). A rather similar conclusion has been reported by Freund et al.[22] in their study of the CO adsorption on AuNPs of varying size supported on a FeO(111) film. Similarly, our proposal is in good agreement with the results obtained in a recent high resolution XPS study of CO adsorption on a model Au/CeO_2 sample.[24]

DFT calculations performed both on gold single-crystal surfaces[33,34] and on gold clusters[35] also support this view. They show a strong structure sensitivity for CO adsorption on gold; sites with low coordination number show the highest estimated adsorption energies.

The analysis of the D_{4-j} data (Table 1) also provides us with some quantitative data. Thus, for Au/CTZ, the fraction of the total number of gold atoms responsible for CO adsorption is $D_{4-7}=0.14$, one half of which (0.07) corresponds to surface gold atoms with $CN \leq 6$. In the case of the Au/CZ catalyst, with a narrower particle size distribution and smaller mean particle size, this fraction turns out to be $D_{4-7}=0.48$, the contribution of surface atoms with $CN \leq 6$ being $D_{4-6}=0.26$.

Under the experimental conditions applied in this work, the surface saturation of the supported AuNPs is reached

when CO is adsorbed on sites with a well-defined structure, and specifically on those with $CN \leq 7$. This conclusion contrasts with that drawn in a very recent quantitative study on the CO adsorption on supported gold catalysts, in which defective surface atoms with rather ill-defined nanostructural properties are considered to be involved.[21]

In accordance with our proposal, the loss of CO adsorption capability in AuNPs that are larger than 5 nm, which is observed in practice,[36] may be interpreted as being due to the progressive decrease of D_{4-7} and CN_{4-7} that occurs in AuNPs as their size increases. By applying our nanostructural model, the following pairs of D_{4-7} (CN_{4-7}) data could be estimated for particles of 5 nm: 0.10 (0.31), 10 nm: 0.03 (0.17), and 15 nm: 0.01 (0.09). As others have also stressed,[17,22] this geometric factor, rather than size-related changes in the electronic structure of the AuNPs, or modifications occurring in the distribution of not well-defined defective sites, could explain the very low CO adsorption capability of such large particles.

Despite the exceptional agreement found between the experimental CO adsorption data and the predictions resulting from the application of our nanostructural model, which is actually based on the chemical principles allowing interpretation of the CO adsorption data recorded at much lower temperatures and P_{CO} values on model single crystal surfaces,[12,18] some difference between the thermodynamic properties of CO adsorbed on single crystal surfaces and highly dispersed AuNPs may be expected to occur. As a number of earlier studies[18,22,23] have shown, the heat of CO adsorption on AuNPs grows as the particle size diminishes. This effect would obviously determine the precise T and P(CO) values required to reach the surface saturation in experiments on powdered supported gold catalysts. The influence of the support on the chemisorptive properties of the corresponding dispersed AuNPs might also be analyzed in similar terms. Support effects would most likely be reflected in modifications of the adsorption enthalpy, and/or eventually, in nanoparticle morphology and size distribution.

Though based on an experimental approach other than that followed herein, attempts at correlating nanostructural properties of supported gold phases and catalytic activity for CO oxidation have been reported.[30,37] To our knowledge, however, no similar correlations involving CO adsorption data have been established to date. The lack of quantitative data for CO adsorption on supported gold phases is probably a major reason justifying the absence of such correlations.

In summary, by combining experimental STEM-HAADF, HREM, and volumetric adsorption studies with nanostructural modeling techniques, a powerful tool for interpreting and even predicting the quantitative CO adsorption on supported gold catalysts has been developed. The adsorption experiments were run under CO partial-pressure and temperature conditions that were significantly higher than those usually applied in studies on model single crystal surfaces. Our results show, however, that the nature of the surface sites involved in both studies are essentially the same, thus bridging the T and P_{CO} gap existing between them. Moreover, our approach does also provide us with a powerful tool for analyzing several other very relevant nanostructural features of supported gold catalysts. Such is the case of the number of surface sites with a specific coordination number, or the number and geometric environment of metal atoms located at the perimeter of the AuNPs. This information may be critically important for discussing the relationship existing between nanostructure and catalytic behavior in supported gold systems on a sounder basis.

Experimental Section

Two catalysts were investigated: 2.5 wt % Au/$Ce_{0.62}Zr_{0.38}O_2$ (Au/CZ), with a BET surface area of 63 $m^2 g^{-1}$, and 1.5 wt % Au/$Ce_{0.50}Tb_{0.12}Zr_{0.38}O_{2-x}$ (Au/CTZ), with a BET surface area of 16 $m^2 g^{-1}$. The mixed-oxide supports were kindly donated by Grace Davison. The gold precursor was 99.99 % H[$AuCl_4$], from Alfa Aesar. The catalysts were prepared by deposition-precipitation methods; aqueous solutions of sodium carbonate (Au/CZ) and urea (Au/CTZ) were used as precipitating agents. Details of the preparation procedure are reported in ref. [38] (Au/CZ) and ref. [19] (Au/CTZ). The metal loadings were confirmed by ICP analysis.

Ultra-high-resolution high-angle annular dark-field scanning transmission electron microscopy images were recorded on a probe-aberration-corrected FEI Titan 80 300 kV microscope at CEA Grenoble, which uses a sub-angstrom-size electron probe. High-resolution electron microscopy images were recorded in a JEOL2010F 200 kV microscope with 0.19 nm spatial resolution. AuNPs used as models in our HREM image simulation studies, and in the structural analysis of the experimental AuNP size distributions, were built with RHODIUS, a computer program developed at our laboratory.

Received: June 23, 2009
Revised: November 25, 2009
Published online: February 23, 2010

Keywords: adsorption · carbon monoxide · gold · supported catalysts · surface analysis

[1] G. C. Bond, D. T. Thompson, *Gold Bull.* **2000**, *33*, 41 – 50.
[2] F. Boccuzzi, A. Chiorino, M. Manzoli, P. Lu, T. Akita, S. Ichikawa, M. Haruta, *J. Catal.* **2001**, *202*, 256 – 267.
[3] J. C. Clark, S. Dai, S. H. Overbury, *Catal. Today* **2007**, *126*, 135 – 142.
[4] D. Widmann, R. Leppelt, R. J. Behm, *J. Catal.* **2007**, *251*, 437 – 442.
[5] W. Deng, M. Flytzani-Stephanopoulos, *Angew. Chem.* **2006**, *118*, 2343 – 2347; *Angew. Chem. Int. Ed.* **2006**, *45*, 2285 – 2289.
[6] W. Deng, J. D. Jesus, H. Saltsburg, M. Flytzani-Stephanopoulos, *Appl. Catal. A* **2005**, *291*, 126 – 135.
[7] D. L. Trimm, *Appl. Catal. A* **2005**, *296*, 1 – 11.
[8] R. Burch, *Phys. Chem. Chem. Phys.* **2006**, *8*, 5483 – 5500.
[9] A. Abd El Moemen, A. Karpenko, Y. Denkwitz, R. J. Behm, *J. Power Sources* **2009**, *190*, 64 – 75.
[10] A. Amieiro Fonseca, J. M. Fisher, D. Ozkaya, M. D. Shannon, D. Thompsett, *Top. Catal.* **2007**, *44*, 223 – 235.
[11] J. Kim, E. Samano, B. E. Koel, *J. Phys. Chem. B* **2006**, *110*, 17512 – 17517.
[12] D. C. Meier, V. Bukhtiyarov, D. W. Goodman, *J. Phys. Chem. B* **2003**, *107*, 12668 – 12671.
[13] J. M. Gottfried, K. J. Schmidt, S. L. M. Schroeder, K. Christmann, *Surf. Sci.* **2003**, *536*, 206 – 224.
[14] C. Ruggiero, P. Hollins, *Surf. Sci.* **1997**, *583*, 377 – 379.
[15] M. Mavrikakis, P. Stoltze, J. Norskov, *Catal. Lett.* **2000**, *64*, 101 – 106.

[16] Z. P. Liu, P. Hu, A. Alavi, *J. Am. Chem. Soc.* **2002**, *124*, 14770 – 14779.
[17] T. V. W. Janssens, B. S. Clausen, B. Hvolbaek, H. Falsig, C. H. Christensen, T. Bligaard, J. K. Norskov, *Top. Catal.* **2007**, *44*, 15 – 26.
[18] R. Meyer, C. Lemire, Sh. K. Shaikhutdinov, H. J. Freund, *Gold Bull.* **2004**, *37*, 72 – 124.
[19] S. E. Collins, J. M. Cíes, E. del Río, M. López-Haro, S. Trasobares, J. J. Calvino, J. M. Pintado, S. Bernal, *J. Phys. Chem. C* **2007**, *111*, 14371 – 14379.
[20] F. Menegazzo, M. Manzoli, A. Chiorino, F. Boccuzzi, T. Tabakova, M. Signoretto, F. Pinna, N. Pernicone, *J. Catal.* **2006**, *237*, 431 – 434.
[21] A. Chiorino, M. Manzoli, F. Menegazzo, M. Signoretto, F. Vindigni, F. Pinna, F. Boccuzzi, *J. Catal.* **2009**, *262*, 169 – 176.
[22] C. Lemire, R. Meyer, Sh. K. Shaikhutdinov, H. J. Freund, *Surf. Sci.* **2004**, *552*, 27 – 34.
[23] D. C. Meier, D. W. Goodman, *J. Am. Chem. Soc.* **2004**, *126*, 1892 – 1899.
[24] C. J. Weststrate, A. Resta, R. Westerström, E. Lundgren, A. Mikkelsen, J. N. Andersen, *J. Phys. Chem. C* **2008**, *112*, 6900 – 6906.
[25] S. J. Pennycook, D. E. Jesson, *Ultramicroscopy* **1991**, *37*, 14 – 38.
[26] A. H. Janssen, C.-M. Yang, Y. Wang, F. Schth, A. J. Koster, K. P. de Jong, *J. Phys. Chem. B* **2003**, *107*, 10552 – 10556.
[27] J. M. Thomas, P. A. Midgley, T. J. V. Yates, J. S. Barnard, R. Raja, I. Arslan, M. Weyland, *Angew. Chem.* **2004**, *116*, 6913 – 6915; *Angew. Chem. Int. Ed.* **2004**, *43*, 6745 – 6747.
[28] A. A. Herzing, C. J. Kiely, A. F. Carley, P. Landon, G. J. Hutchings, *Science* **2008**, *321*, 1331 – 1335.
[29] P. D. Nellist, S. J. Pennycook, *Science* **1996**, *274*, 413 – 415.
[30] A. Carlsson, A. Puig-Molina, T. V. W. Janssens, *J. Phys. Chem. B* **2006**, *110*, 5286 – 5293.
[31] J. C. González, J. C. Hernández, M. López-Haro, E. del Río, J. J. Delgado, A. B. Hungría, S. Trasobares, S. Bernal, P. A. Midgley, J. J. Calvino, *Angew. Chem.* **2009**, *121*, 5417 – 5419; *Angew. Chem. Int. Ed.* **2009**, *48*, 5313 – 5315.
[32] J. P. den Breejen, P. B. Radstake, G. L. Bezemer, J. H. Bitter, V. Frøseth, A. Holmen, K. P. de Jong, *J. Am. Chem. Soc.* **2009**, *131*, 7197 – 7203.
[33] D. Loffreda, P. Sautet, *J. Phys. Chem. B* **2005**, *109*, 9596 – 9603.
[34] A. Hussain, D. Curulla Ferré, J. Gracia, B. E. Nieuwenhuys, J. W. Niemantsverdriet, *Surf. Sci.* **2009**, *603*, 2734 – 2741.
[35] E. M. Fernández, P. Ordejón, L. C. Balbás, *Chem. Phys. Lett.* **2005**, *408*, 252 – 257.
[36] M. Haruta, *Catal. Today* **1997**, *36*, 153 – 166.
[37] T. V. W. Janssens, A. Carlsson, A. Puig-Molina, B. S. Clausen, *J. Catal.* **2006**, *240*, 108 – 113.
[38] A. Goguet, R. Burch, Y. Chen, C. Hardacre, P. Hu, R. W. Joyner, F. C. Meunier, B. S. Mun, D. Thompsett, D. Tibiletti, *J. Phys. Chem. C* **2007**, *111*, 16927 – 16933.

